

Study of K_S semileptonic decays and \mathcal{CPT} test with the KLOE detector

Daria Kamińska
on behalf of the KLOE-2 Collaboration

The Marian Smoluchowski Institute of Physics, Jagiellonian University
 Łojasiewicza 11, 30-348 Kraków, Poland

E-mail: daria.kaminska@doctoral.uj.edu.pl

Abstract. Study of semileptonic decays of neutral kaons allows to perform a test of discrete symmetries, as well as basic principles of the Standard Model. In this paper a general review on dependency between charge asymmetry constructed for semileptonic decays of short- and long-lived kaons and \mathcal{CPT} symmetry is given. The current status of determination of charge asymmetry for short-lived kaon, obtained by reconstruction of about 10^5 $K_S \rightarrow \pi e \nu$ decays collected at DAΦNE with the KLOE detector is also reviewed.

1. Introduction

Discrete symmetries of nature such as charge conjugation (\mathcal{C}), parity (\mathcal{P}) or time reversal (\mathcal{T}) do not lead to new conserved quantities. Nevertheless, all of the mentioned symmetries plays an important role in particle physics, especially in calculations of the cross sections and decay rates. Weak interaction does not conserve the \mathcal{C} , \mathcal{P} , \mathcal{T} or combined \mathcal{CP} symmetry. However, up to now, there is no indication of \mathcal{CPT} symmetry violation [1], which would also imply the break of Lorentz symmetry [2]. A special role in \mathcal{CPT} violation searches plays a neutral kaon system which, due to a sensitivity to a variety of symmetry violation effects, is one of the best candidates for such kind of studies. One of the possible tests is based on comparison between semileptonic asymmetry in K_S decays (A_S) and the analogous asymmetry in K_L decays (A_L).

2. Test of \mathcal{CPT} symmetry violation through semileptonic decays in neutral kaon system

2.1. Semileptonic decays in neutral kaon system

Neutral kaons are the lightest particles which contain a strange quark. Observed short-lived K_S and long-lived K_L are linear combinations of strange eigenstates (K^0 and \bar{K}^0):

$$\begin{aligned} |K_L\rangle &= \frac{1}{\sqrt{2(1+|\epsilon_L|^2)}} \left((1+\epsilon_L) |K^0\rangle - (1-\epsilon_L) |\bar{K}^0\rangle \right), \\ |K_S\rangle &= \frac{1}{\sqrt{2(1+|\epsilon_S|^2)}} \left((1+\epsilon_S) |K^0\rangle + (1-\epsilon_S) |\bar{K}^0\rangle \right), \end{aligned} \tag{1}$$

where introduced small parameters ϵ_L and ϵ_S can be rewritten to separate \mathcal{CP} and $\mathcal{CP}\mathcal{T}$ violation parameters ϵ_K and δ_K , respectively:

$$\begin{aligned}\epsilon_S &= \epsilon_K + \delta_K, \\ \epsilon_L &= \epsilon_K - \delta_K.\end{aligned}\quad (2)$$

In this paper a particular emphasis will be given to semileptonic decays of K-short and K-long states ($K_{S/L} \rightarrow \pi e \nu$). According to Eq. 1, only the four possible decays of strange eigenstates should be considered:

$$\begin{aligned}K^0 &\rightarrow \pi^- e^+ \nu, & K^0 &\rightarrow \pi^+ e^- \bar{\nu}, \\ \bar{K}^0 &\rightarrow \pi^+ e^- \bar{\nu}, & \bar{K}^0 &\rightarrow \pi^- e^+ \nu.\end{aligned}\quad (3)$$

However, in the Standard Model the decay of K^0 (or \bar{K}^0) state is associated with the transition of the \bar{s} quark into \bar{u} quark (or s into u) and emission of the charged boson. Change of strangeness (ΔS) implies the corresponding change of electric charge (ΔQ) (see Figure 1). This is so called $\Delta S = \Delta Q$ rule. Therefore, decays of $K^0 \rightarrow \pi^- e^+ \nu$ and $\bar{K}^0 \rightarrow \pi^+ e^- \bar{\nu}$ are present but $K^0 \rightarrow \pi^+ e^- \bar{\nu}$ and $\bar{K}^0 \rightarrow \pi^- e^+ \nu$ are forbidden by if $\Delta Q = \Delta S$.

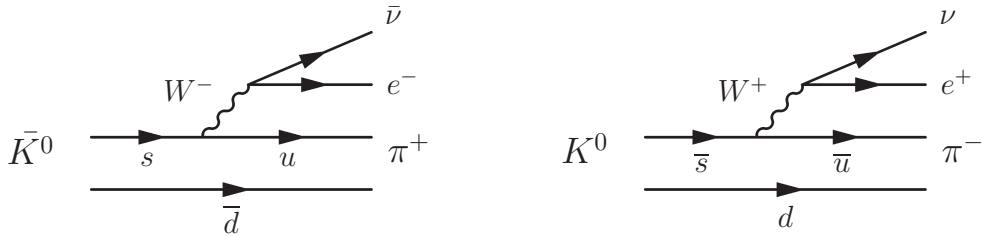


Figure 1. Feynman diagrams for K^0 and \bar{K}^0 semileptonic decay.

Decay amplitudes for semileptonic decays of states $|K^0\rangle$ and $|\bar{K}^0\rangle$ can be written as follows [3]:

$$\begin{aligned}\langle \pi^- e^+ \nu | H_{weak} | K^0 \rangle &= \mathcal{A}_+, & \langle \pi^+ e^- \bar{\nu} | H_{weak} | \bar{K}^0 \rangle &= \bar{\mathcal{A}}_-, \\ \langle \pi^+ e^- \bar{\nu} | H_{weak} | K^0 \rangle &= \mathcal{A}_-, & \langle \pi^- e^+ \nu | H_{weak} | \bar{K}^0 \rangle &= \bar{\mathcal{A}}_+, \end{aligned}\quad (4)$$

where the H_{weak} is the term of Hamiltonian corresponding to the weak interaction and $\mathcal{A}_+, \bar{\mathcal{A}}_-, \mathcal{A}_-, \bar{\mathcal{A}}_+$ parametrize the semileptonic decay amplitudes.

It is useful to introduce the following notation:

$$\begin{aligned}x &= \frac{\bar{\mathcal{A}}_+}{\mathcal{A}_+}, & \bar{x} &= \left(\frac{\mathcal{A}_-}{\bar{\mathcal{A}}_-} \right)^*, & y &= \frac{\bar{\mathcal{A}}_-^* - \mathcal{A}_+}{\bar{\mathcal{A}}_-^* + \mathcal{A}_+}, \\ x_{\pm} &= \frac{x \pm \bar{x}^*}{2} = \frac{1}{2} \left[\frac{\bar{\mathcal{A}}_+}{\mathcal{A}_+} \pm \left(\frac{\mathcal{A}_-}{\bar{\mathcal{A}}_-} \right)^* \right].\end{aligned}\quad (5)$$

For further considerations, rules for applying symmetry operators to amplitudes of two spin zero systems A and B (and corresponding anti-systems \bar{A} and \bar{B}) could be summarized as:

$$\begin{aligned}\langle \mathcal{TB} | \mathcal{T} H_{wk} \mathcal{T}^{-1} | \mathcal{TA} \rangle &= (\langle \mathcal{B} | \mathcal{T} H_{wk} \mathcal{T}^{-1} | \mathcal{A} \rangle)^* \\ \langle \mathcal{CPB} | \mathcal{CP} H_{wk} \mathcal{CP}^{-1} | \mathcal{CPA} \rangle &= \langle \bar{\mathcal{B}} | \mathcal{CP} H_{wk} \mathcal{CP}^{-1} | \bar{\mathcal{A}} \rangle \\ \langle \mathcal{CPTB} | \mathcal{CPT} H_{wk} \mathcal{CPT}^{-1} | \mathcal{CPTA} \rangle &= (\langle \bar{\mathcal{B}} | \mathcal{CPT} H_{wk} \mathcal{CPT}^{-1} | \bar{\mathcal{A}} \rangle)^*\end{aligned}\quad (6)$$

One obtains the relation between the semileptonic amplitudes and conservation of a particular symmetry by applying the presented above rules to the states presented in Eq. 4. These considerations are summarized in Table 1.

Table 1. Relations between discrete symmetries and semileptonic amplitudes

| Conserved quantity | Required relation |
|----------------------------|--------------------------|
| $\Delta S = \Delta Q$ rule | $x = \bar{x} = 0$ |
| \mathcal{CPT} symmetry | $x = \bar{x}^*, y = 0$ |
| \mathcal{CP} symmetry | $x = \bar{x}, y = Im(y)$ |
| \mathcal{T} symmetry | $y = Re(y)$ |

2.2. Charge asymmetry

Charge asymmetry can be defined for semileptonic decays of K_S and K_L mesons in the following way:

$$A_{S,L} = \frac{\Gamma(K_{S,L} \rightarrow \pi^- e^+ \nu) - \Gamma(K_{S,L} \rightarrow \pi^+ e^- \bar{\nu})}{\Gamma(K_{S,L} \rightarrow \pi^- e^+ \nu) + \Gamma(K_{S,L} \rightarrow \pi^+ e^- \bar{\nu})} \quad (7)$$

and can be rewritten in terms of parameters introduced in Eq. 5:

$$A_{S,L} = 2 [Re(\epsilon_K) \pm Re(\delta_K) - Re(y) \pm Re(x_-)]. \quad (8)$$

In that case, sum and difference of the A_S and A_L allow to search for the \mathcal{CPT} symmetry violation, either in the decay amplitudes through the parameter y or in the mass matrix through the parameter δ_K :

$$\begin{aligned} A_S + A_L &= 4Re(\epsilon) - 4Re(y), \\ A_S - A_L &= 4Re(\delta_K) + 4Re(x_-). \end{aligned} \quad (9)$$

2.3. Experimental verification

The measurement based on 1.9 millions $K_L \rightarrow \pi e \nu$ decays produced in collisions of proton beam with a BeO target performed by KTeV Collaboration allowed to determine A_L values [4]:

$$A_L = (3.322 \pm 0.058_{stat} \pm 0.047_{syst}) \times 10^{-3}. \quad (10)$$

At present most accurate measurement of K_S charge asymmetry was conducted by KLOE experiment. Measurement of A_S was performed with 0.41 fb^{-1} total luminosity data sample and the result is [5]:

$$A_S = (1.5 \pm 9.6_{stat} \pm 2.9_{syst}) \times 10^{-3}. \quad (11)$$

Obtained charge asymmetry for K_S decays is consistent in error limits with charge asymmetry for K_L decays. However, the inaccuracy of K_S determination is more than two orders of magnitude bigger than this of the A_L and the error of A_S is dominated by a statistical uncertainty, which is three times larger than systematical one. Therefore, in this work a new measurement of A_S based on around four times bigger data sample collected by means of the KLOE detector in 2004 and 2005, is presented.

3. The K LOng Experiment at DAΦNE

KLOE was mounted at DAΦNE collider in 1999 and collected data during two campaigns in 2001-2002 and 2004-2005. The gathered data sample corresponds to the total luminosity of 2.5 fb^{-1} . Energy of colliding beams (e^- and e^+) was set to the mass of ϕ meson. DAΦNE collider produce ~ 1300 kaon pairs per second which corresponds to the luminosity $5 \times 10^{32} \text{ cm}^{-2}\text{s}^{-1}$. In order to obtain efficient detection of the K_L mesons the KLOE detector was constructed with a view to properties of neutral kaon system. A schematic cross-section side view of the KLOE detector is shown in Figure 2. The main components of KLOE are the cylindrical drift chamber and the

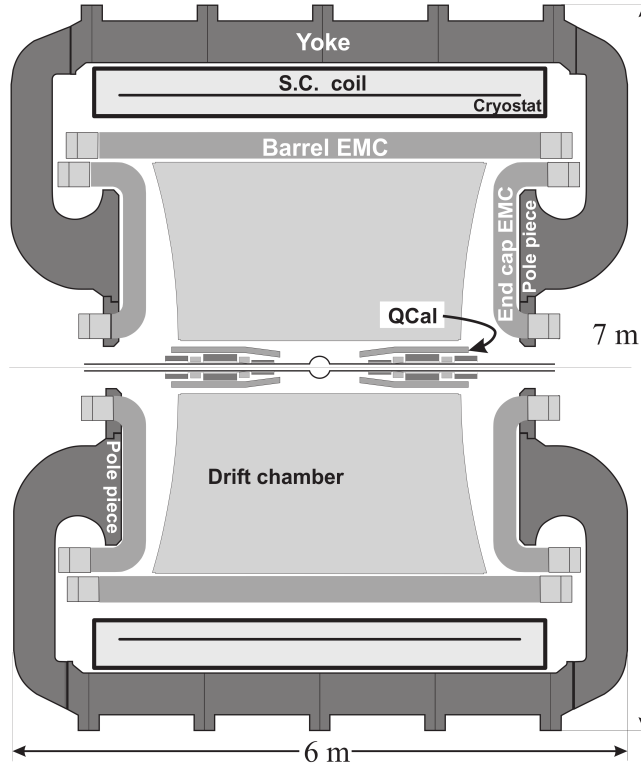


Figure 2. Scheme of the KLOE detector system. Drift chamber in the central part of the KLOE detector is surrounded by the electromagnetic calorimeter. Both detectors are inserted in a magnetic field. Figure adapted from [6].

calorimeter, both surrounding the beam pipe. All elements are immersed in a 0.52 T magnetic field created by superconducting coils that are placed along the beam axis.

The KLOE drift chamber (DC) is a 3.3 m long cylinder with an internal and external radii of 25 cm and 2 m, respectively, which allows to register about 40% of K_L decays inside the chamber while the rest reach the electromagnetic calorimeter. Between the endplates around 12500 sense wires are stretched and allows to obtain: a spatial resolution in the r, φ plane better than 200 μm , a resolution along the z axis of ~ 2 mm and on the resolution of the decay vertex determination of ~ 1 mm. Moreover, the curvature of the reconstructed tracks allows to determine the particle momentum with a relative accuracy of 0.4 %. The drift chamber allows to reconstruct information about charged particles while the calorimeter enables recording of both charged and neutral particles. The KLOE calorimeter has been designed to have an excellent accuracy of energy determination and time resolution:

$$\frac{\sigma(E)}{E} = \frac{5.4\%}{\sqrt{E[\text{GeV}]}} \quad (12)$$

$$\sigma_t = \frac{54 \text{ ps}}{\sqrt{E[\text{GeV}]}} \oplus 140 \text{ ps}$$

in order to register the hits of neutral particles and provide a possibility of the Time of Flight (TOF) measurement.

4. Registration of the $\phi \rightarrow K_L K_S \rightarrow K_L \pi e \nu$ processes at KLOE

4.1. Preselection

Due to the conservation of quantum numbers during decay of ϕ meson the neutral kaons are produced in pairs. In general case it is an entangled anti-symmetric state, which properties allows to perform a fundamental tests of Quantum Mechanics and Lorentz symmetry [7]:

$$|\phi\rangle = \frac{\sqrt{(1+|\epsilon_S|^2)(1+|\epsilon_L|^2)}}{\sqrt{2}(1-\epsilon_S\epsilon_L)} (|K_L(\vec{p})\rangle |K_S(-\vec{p})\rangle - |K_S(\vec{p})\rangle |K_L(-\vec{p})\rangle) \quad (13)$$

where \vec{p} is a momentum in the ϕ meson rest frame. However, when one of the kaon is detected at time $t \gg \tau_s$, the state in Eq. 13 factorizes and the system behaves as if the initial state was a mixture of $|K_L(\vec{p})\rangle |K_S(-\vec{p})\rangle$ and $|K_S(\vec{p})\rangle |K_L(-\vec{p})\rangle$. Hence the detection of K_L at large distance from Interaction Point tags K_S state in the opposite direction. Measurement described in this paper is based on identification of K_S through the detection of K_L interaction in the calorimeter. A sketch of typical signal event is shown in Figure 3(left). Selection of K_L candidates takes into account only clusters with high energy deposition and requires that the cluster is not close to any track reconstructed in the drift chamber. Also, velocity of neutral particle that deposits energy in this cluster must be close to the theoretical value of K_L meson velocity in the ϕ meson rest frame ($\beta \sim 0.22$).

In the next step, candidates for K_S meson decays are selected by selection of two oppositely charged particles with tracks forming a vertex close to the interaction point (IP):

$$\begin{aligned} \rho_{vtx} &< 15 \text{ cm}, \\ |z_{vtx}| &< 10 \text{ cm}, \end{aligned} \quad (14)$$

where $\rho_{vtx} = \sqrt{x_{vtx}^2 + y_{vtx}^2}$. Obtained distribution is shown in Figure 3(right). Then, the rejection of main source of background ($K_S \rightarrow \pi^+ \pi^-$) is conducted by applying the following cuts:

- $70^\circ < \alpha < 175^\circ$
where α is an angle between charged secondaries in K_S rest frame. Obtained α distribution is shown at the left side of Figure 4. In case of three body decay ($K_S \rightarrow \pi e \nu$) it is spanned over a large angle range.
- $300 < M_{inv} < 490 \text{ MeV}$
an invariant mass M_{inv} is calculated using momenta of the particles which tracks form a vertex assuming that both particle were pions. Obtained M_{inv} distribution is shown at the right side of Figure 4.

Both tracks reconstructed in the drift chamber must be associated with neighbouring clusters in calorimeter in order to use Time-of-Flight technique.

4.2. $K_S \rightarrow \pi e \nu$ events identification

The Time of Flight technique aims at rejection of the background, which at this stage of analysis is due to $K_S \rightarrow \pi^+ \pi^-$ events, and at identification of the final charge states ($\pi^\pm e^\mp$). For each particle, the difference δ_t between the measured time of associated cluster (t_{cl}) and expected time of flight is calculated assuming a given mass hypothesis, m_x :

$$\begin{aligned} \delta_t(m_x) &= t_{cl} - \frac{L}{c \cdot \beta(m_x)}, \\ \beta(m_x) &= \frac{P}{\sqrt{P^2 + m_x^2}}, \end{aligned} \quad (15)$$

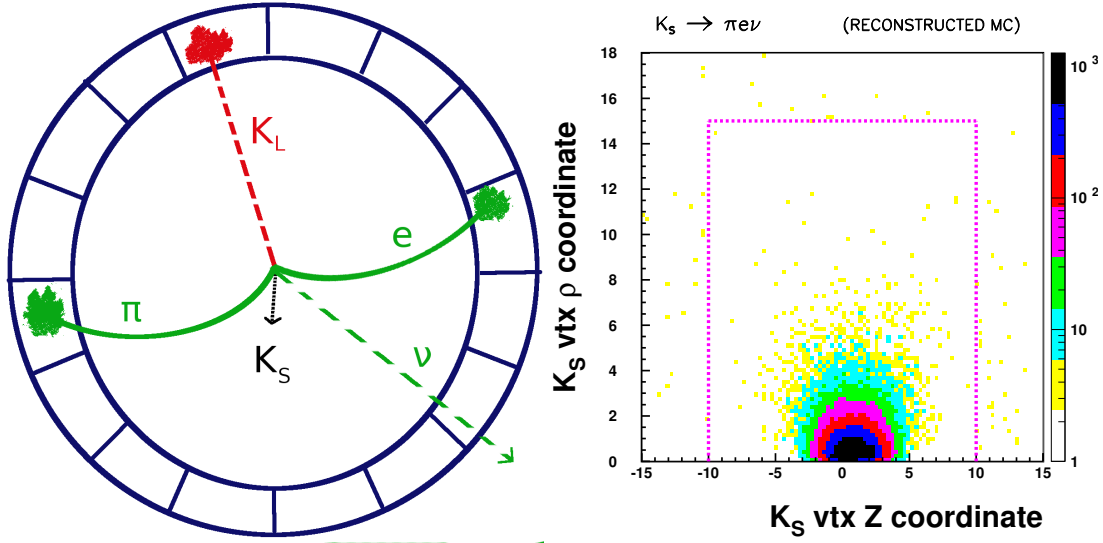


Figure 3. Left: Transverse view of exemplary signal event. The K_S is identified using the K_L interaction in the calorimeter. In the next step two oppositely charged particle tracks are selected which form a vertex near the interaction point. Both tracks must be associated with the calorimeter clusters. Right: Monte Carlo simulation of transversal and longitudinal coordinates of vertex position for $K_S \rightarrow \pi e \nu$ events. Dashed line represents applied cuts which preserves $\sim 95\%$ of the signal.

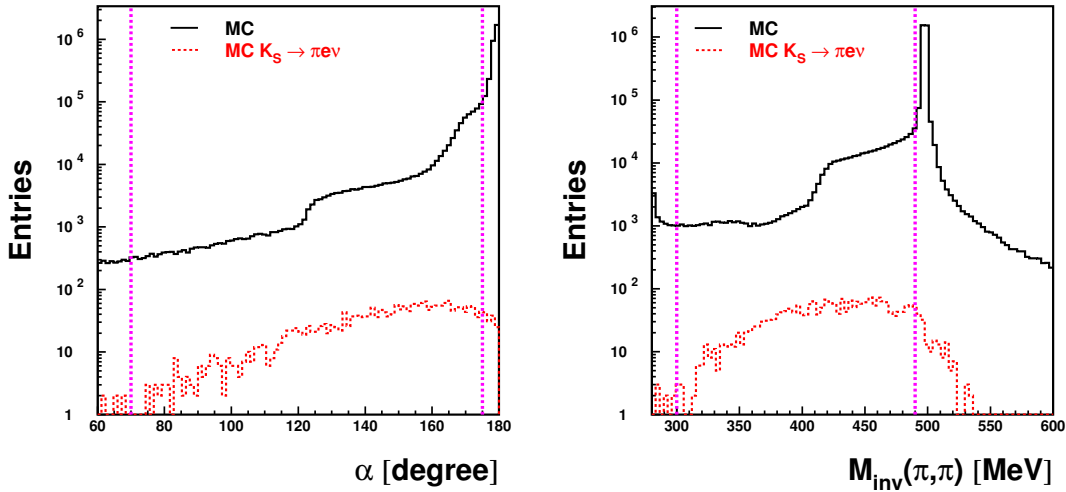


Figure 4. Left: Simulated distribution of angle between charged secondaries in K_S rest frame. Right: Simulated distribution of invariant mass calculated under assumption that both registered particles were pions. In both figures solid and dashed histograms represents all events and semileptonic decays, respectively. Vertical dashed lines represent cuts described in text.

where L is a total length of particle trajectory and P is particle momentum. For further consideration it is useful to introduce the difference of $\delta_t(m_a)$ and $\delta_t(m_b)$:

$$d\delta_{t,ab} = \delta_t(m_a)_1 - \delta_t(m_b)_2. \quad (16)$$

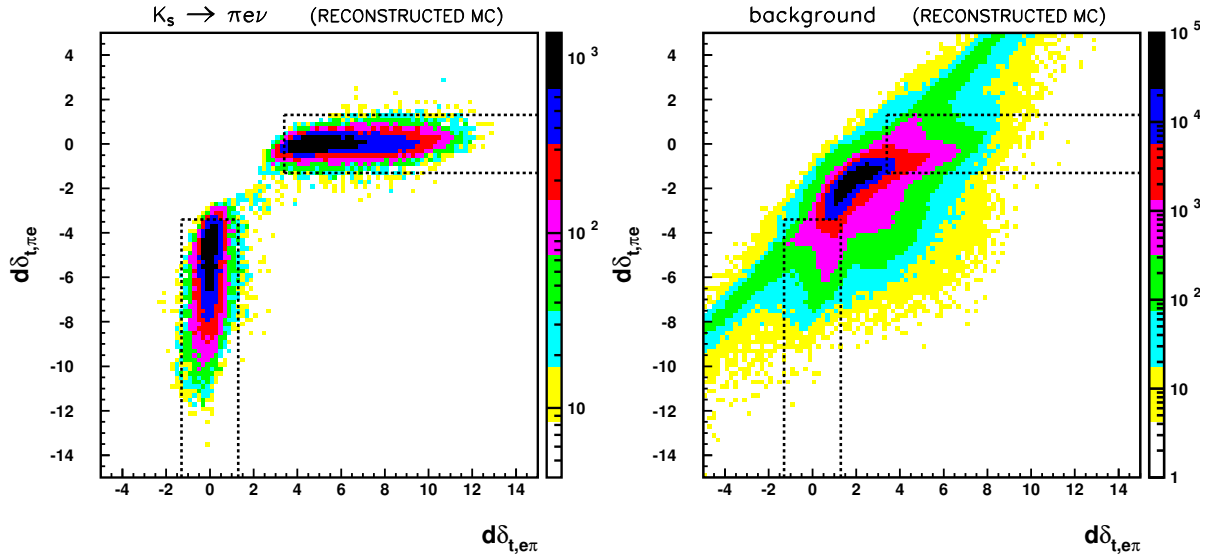


Figure 5. Simulated distributions of time differences $d\delta_{t,\pi e}$ vs $d\delta_{t,e\pi}$ defined in Eq. 18 for $K_S \rightarrow \pi e \nu$ events (left) and background events (right), once the $\delta_{t,\pi\pi}$ cut has been applied. The regions delimited by the dashed lines are selected. In case of $e\pi$ (πe) the $d\delta_{t,e\pi}$ ($d\delta_{t,\pi e}$) variable acquires value close to zero.

where suffix 1 and 2 refers to the first and second particle according to the ordering determined by the reconstruction procedure.

Two cuts are further applied. For the first cut, both particles are assumed to be pions and $d\delta_{t,\pi\pi}$ is calculated. For $K_S \rightarrow \pi\pi$ events this value is around zero and this fraction of events could be rejected by requiring:

$$|d\delta_{t,\pi\pi}| > 1.5 \text{ ns.} \quad (17)$$

Then, for surviving events, the pion-electron hypothesis is tested:

$$\begin{aligned} d\delta_{t,\pi e} &= \delta_t(m_\pi)_1 - \delta_t(m_e)_2, \\ d\delta_{t,e\pi} &= \delta_t(m_e)_1 - \delta_t(m_\pi)_2. \end{aligned} \quad (18)$$

If a mass assumption is correct then one of the variables above should be close to zero. The obtained Monte Carlo distributions for $K_S \rightarrow \pi^\pm e^\mp \nu$ and background events are presented in Figure 5. Hence, the following cut is applied:

$$\begin{aligned} |d\delta_{t,e\pi}| < 1.3 \text{ ns} \wedge d\delta_{t,\pi e} < -3.4 \text{ ns} \\ \text{or} \\ d\delta_{t,e\pi} > 3.4 \text{ ns} \wedge |d\delta_{t,\pi e}| < 1.3 \text{ ns} \end{aligned} \quad (19)$$

The above requirement ensures that the possibility of misidentification of charged particles from signal events is equal to 10^{-4} only.

Obtained distributions for simulated data and experimental KLOE data are shown in Figure 6 (top). The Monte Carlo simulation indicates the signal position around the point (0,0) while the background location is spread at the corners of the obtained distribution. Due to that an additional TOF cut is applied by selecting events within the circle in the $\delta_t(e)$ vs $\delta_t(\pi)$

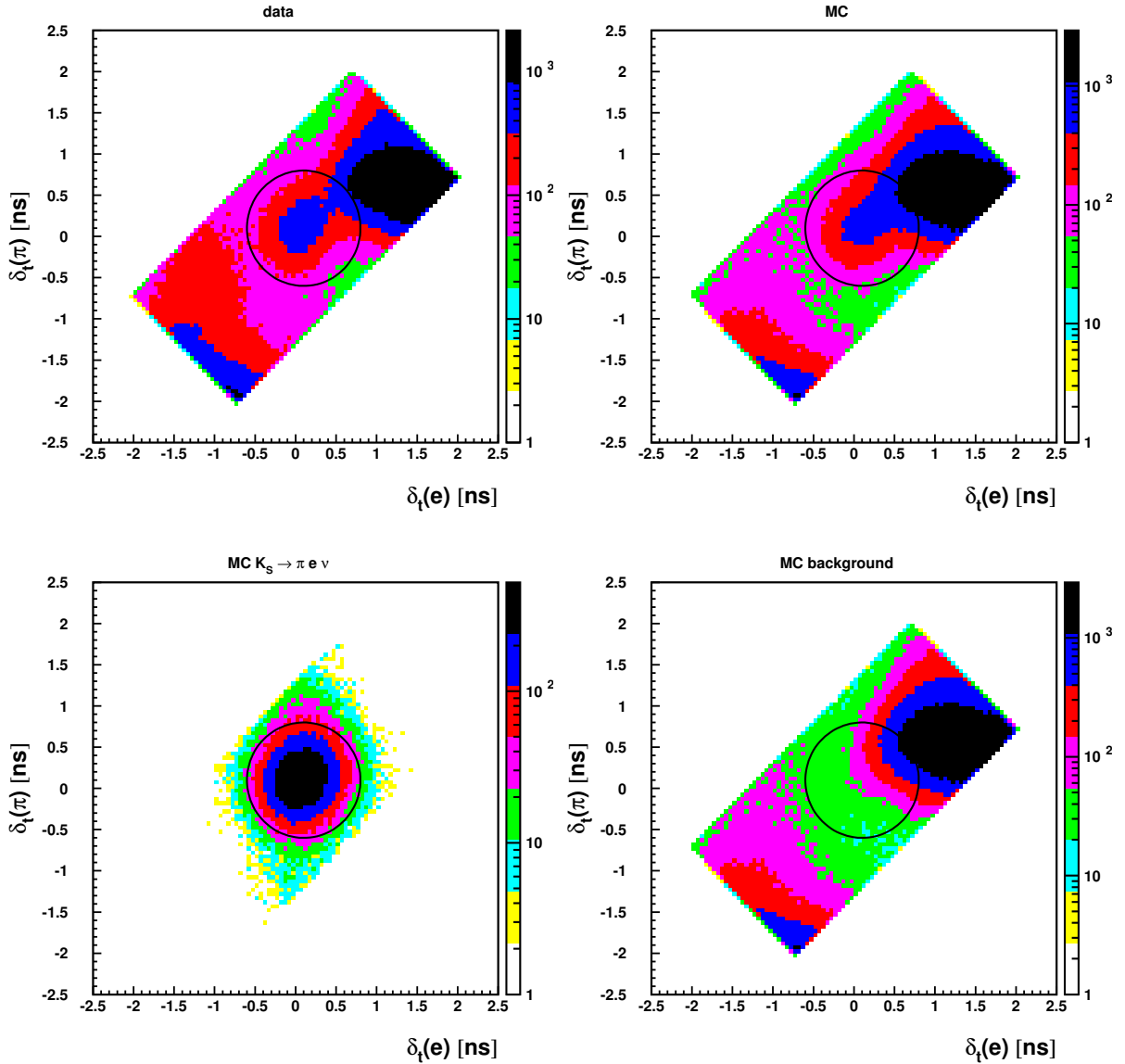


Figure 6. Distributions of the time difference for pion mass hypothesis ($\delta_t(\pi)$) versus the time difference for electron mass hypothesis ($\delta_t(e)$) for experimental data (top-left), total MC events (top-right), MC $K_S \rightarrow \pi e \nu$ events (bottom-left) and MC background events (bottom-right). Events within the circle are retained for further analysis.

plane, as shown in Figure 6. This cut allows to preserve 94% of the remaining signal and control the number of selected background events for normalization. The distribution of the difference between the missing energy and momentum ($\Delta E(\pi, e)$) shows the remaining background components (see Figure 7). Based on an integrated luminosity of 1.7fb^{-1} around 10^5 of $K_S \rightarrow \pi e \nu$ decays were reconstructed and will be used to determine the charge asymmetry and branching ratio for K_S semileptonic decays. A preliminary analysis shows a potential of reaching a two times better statistical error determination with a sample four times bigger than the previous KLOE analysis. The analysis is still in progress and preliminary results will be available soon.

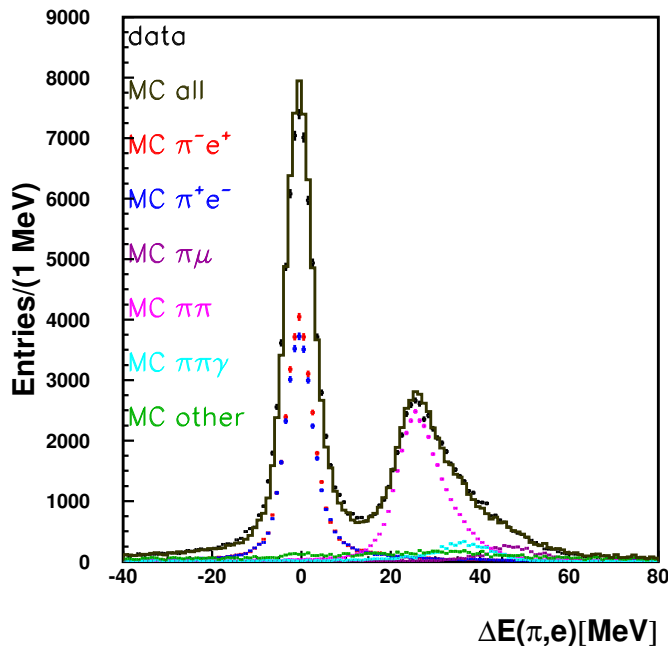


Figure 7. Distribution of $\Delta E(\pi, e) = E_{miss} - p_{miss}$ for all selected events after normalization procedure.

5. KLOE-2 Project

DAΦNE collider in previous years was adapted to increased delivered luminosity by installation of the new interaction region based on the Crabbed Waist compensation together with large Piwinski angle [10]. Those changes should increase by factor of three the amount of the delivered luminosity with respect to the performance reached before. Together with the upgrade of the KLOE detector this will allow to collect by KLOE-2 project the order of 10 fb^{-1} of integrated luminosity. The detector itself was equipped with crystal (CCALT) [11] and tile (QCALT) [12] calorimeters which covers the low polar angles and improve the detection of the photons that are coming from K_L decays in the drift chamber, respectively. Also, there were mounted the two pairs of small angle tagging devices that allows to detect the low (Low Energy Tagger [13]) and high (High Energy Tagger [14]) energy e^+e^- originated from $e^+e^- \rightarrow e^+e^-X$ reactions. However, the especially important for studies of \mathcal{CPT} symmetry violation through semileptonic decays in neutral kaons is precise reconstruction of tracks momenta and vertex reconstruction close to the Interaction Point. This will be provided by Inner Tracker detector made out in a novel GEM technology [15]. Those upgrades will also improve the sensitivity of \mathcal{CPT} and Lorentz invariance tests, which were presented by the KLOE experiment and became the most precise measurement of the \mathcal{CPT} violating parameters Δa_μ for neutral kaons in the Standard Model Extension (SME) [16]. Measured values of Δa_μ currently have a precision of 10^{-18} GeV and are proportional to the parameter δ_K [17, 18, 19].

It should be emphasised that KLOE-2 aims to significantly improve the sensitivity of tests of discrete symmetries, through studies of K_S charge asymmetry or quantum interferometry effects in the kaon decays, beyond the presently achieved results.

Acknowledgments

We warmly thank our former KLOE colleagues for the access to the data collected during the KLOE data taking campaign. We thank the DAΦNE team for their efforts in maintaining low background running conditions and their collaboration during all data taking. We want to thank our technical staff: G.F. Fortugno and F. Sborzacchi for their dedication in ensuring efficient operation of the KLOE computing facilities; M. Anelli for his continuous attention to the gas system and detector safety; A. Balla, M. Gatta, G. Corradi and G. Papalino for electronics maintenance; M. Santoni, G. Paoluzzi and R. Rosellini for general detector support; C. Piscitelli for his help during major maintenance periods. This work was supported in part by the EU Integrated Infrastructure Initiative Hadron Physics Project under contract number RII3-CT- 2004-506078; by the European Commission under the 7th Framework Programme through the ‘Research Infrastructures’ action of the ‘Capacities’ Programme, Call: FP7-INFRASTRUCTURES-2008-1, Grant Agreement No. 227431; by the Polish National Science Centre through the Grants No. DEC-2011/03/N/ST2/02641, 2011/01/D/ST2/00748, 2011/03/N/ST2/02652, 2013/08/M/ST2/0323, DEC-2014/12/S/ST2/00459, 2013/11/B/ST2/04245 and by the Foundation for Polish Science through the MPD programme and the project HOMING PLUS BIS/2011-4/3.

References

- [1] V. A. Kostelecky, N. Russell, *Rev. Mod. Phys.* **83** (2011), 11
- [2] O. W. Greenberg, *Phys. Rev. Lett.* **89** (2002), 231602
- [3] L. Maiani, G. Pancheri, N. Paver, INFN-LNF (1995)
- [4] A. Alavi-Harati et al. (KTeV Collaboration), *Phys. Rev. Lett.* **88** (2002), 181601
- [5] F. Ambrosino et al. (KLOE Collaboration), *Phys. Lett.* **B636** (2006), 173
- [6] G. Vignola, M. Bassetti, M. E. Biagini, C. Biscari, R. Boni, *Conf. Proc.* **C960610** (1996), 22
- [7] G. Amelino-Camelia et al., *Eur. Phys. J.* **C68** (2010), 619
- [8] Adinolfi, M. et al., (KLOE Collaboration), *Nucl. Instrum. Meth.* **A461** (2001), 25
- [9] Adinolfi, M. et al., (KLOE Collaboration), *Nucl. Instrum. Meth.* **A482** (2002), 364
- [10] Milardi, C. et al., (DAΦNE Collaboration), CERN-2008-006 (2008), 1
- [11] M. Cordelli et al., *Nucl. Instrum. Meth.* **A718** (2013), 81
- [12] A. Balla et al., *Nucl. Instrum. Meth.* **A718** (2013), 95
- [13] M. Adinolfi et al., (KLOE Collaboration), *Nucl. Instrum. Meth.* **A617** (2010), 81
- [14] M. Adinolfi et al., (KLOE Collaboration), *Nucl. Instrum. Meth.* **A617** (2010), 266
- [15] G. Morello et al., *JINST* **9** (2013), C01014
- [16] D. Babusci et al., (KLOE Collaboration), *Phys. Lett* **B730** (2014), 89
- [17] D. Colladay and V. A. Kostelecky, *Phys. Rev.* **D55**, (1997) 6760
- [18] D. Colladay and V. A. Kostelecky, *Phys. Rev.* **D58**, (1998) 116002
- [19] V. A. Kostelecky and R. Potting, *Phys. Rev.* **D51**, (1995) 3923